NASA TECHNICAL MEMORANDUM

NASA TM X-73464

NASA TM X-73464

NOISE GENERATED BY IMPINGEMENT OF TURBULENT FLOW ON AIRFOILS OF VARIED CHORD, CYLINDERS, AND OTHER FLOW OBSTRUCTIONS

by W. A. Olsen
Lewis Research Center
Cleveland, Ohio 44135

TECHNICAL PAPER to be presented at Third Aero-Acoustic Conference sponsored by the American Institute of Aeronautics and Astronautics Palo Alto, California, July 20-22, 1976

AIAA Paper No. 76-504

NOISE GENERATED BY IMPINGEMENT OF TURBULENT FLOW ON AIRFOILS OF VARIED CHORD, CYLINDERS, AND OTHER FLOW OBSTRUCTIONS

by W. A. Olsen

Lewis Research Center
Cleveland, Ohio 44135

TECHNICAL PAPER to be presented at

Third Aero-Acoustic Conference sponsored by the
American Institute of Aeronautics and Astronautics
Palo Alto, California, July 20-22, 1976

NATIONAL AERONAUTICS AND SPACE ADMINISTRATION

NOISE GENERATED BY IMPINGEMENT OF TURBULENT FLOW ON AIRFOILS OF VARIED CHORD, CYLINDERS, AND OTHER FLOW OBSTRUCTIONS

by W. A. Olsen

National Aeronautics and Space Administration
Lewis Research Center
Cleveland, Ohio 44135

E-8829

ABSTRACT

Noise spectra were measured in three dimensions for several surfaces immersed in turbulent flow from a jet and over a range of flow conditions. The data are free field and were corrected to remove the small contributions of jet noise, atmospheric attenuation and feedback tones. These broadband data were compared with the results of available theories which are only strictly applicable to simple geometries over a limited range of conditions. The available theories proved to be accurate over the range of flow, chord length, thickness, angle of attack, and surface geometries defined by the experiments. These results apply to the noise generated by fixed surfaces in engine passages, the lifting surfaces of aircraft and also to fan noise.

INTRODUCTION

The primary objective of the work reported herein was to obtain data for the broadband noise generated by the impingement of an airstream upon fixed airfoils of small to "infinite" chord, and cylinders of varied size and shape. The second objective was to compare these data with the results from available analyses. These results can be related to the noise generated by fixed flow obstructions in engine flow passages, fan and compressor noise, and also to the noise generated by the lift augmentation surfaces of STOL aircraft.

Basic theories for the noise emission from surfaces in a turbulent airstream exist for only a few very simple surface geometries (see fig. 1). These are described in reference 1, which contains a systematic discussion of these theories. The shape of radiation pattern of the overall sound pressure level is predicted in reference 1, but equations to predict the complete noise emission (spectra, radiation pattern, and absolute level) are only given for the small chord airfoil. These theories only apply to a limited range of parameters and geometrical variations. For example, the theory for the small airfoil requires that the chord and thickness of the airfoil be small. The comparisons in this paper between the theoretical results and the data for airfoils of varied chord and thickness will help quantify what small means; and any shortcomings of the theories described in reference 1 will also be shown.

In order to compare the data with theoretical predictions the assumptions required by the theory must be adequately satisfied. Many previous experiments had strong feedback tones (e.g. refs. 2, 3, and 4) which make it difficult to extract the broadband spectra. In other experiments the test surface was in a duct (e.g., ref. 5), which strongly affected the shape of the radiation pattern and spectra. In many experiments, including the one reported herein, the obstruction was immersed in a finite turbulent jet. A large free-jet wind tunnel with screens can give a large region of uniform flow but at the price of more jet noise contamination, which would restrict the frequency and velocity range of the uncontaminated data (e.g., ref. 6). In addition the spatial range of the data would be restricted. Another problem with many experiments is that the range of geometries and parameters covered were limited.

The surfaces tested and discussed herein are airfoils of small (1.0 cm chord) to "infinite" chord and of varied thickness and shape, and also cylinders of varied size and cross sectional shape. These were immersed in the turbulent airstream of a nozzle. The complete three dimensional noise emission from these geometries was measured over a large range of flow conditions. The data were not adversely affected by the experimental problems previously mentioned. These data were compared to the results of the available basic theories in order to determine the validity and limitations of applying the available theories.

DISCUSSION OF AVAILABLE THEORY

Consider turbulent flow over a stationary surface in an otherwise infinite uniform medium at rest. Noise at far field position $\vec{x}$ from a source in the turbulent flow at $\vec{y}$, is proportional to the rms of the density perturbation. The density perturbation is given by equation (1), which was derived in reference 1 by the acoustic analogy approach of Lighthill.

$$\rho'(\vec{x},t) = \frac{1}{c_0^2}\left[\int_T\int_V \frac{\partial^2 G}{\partial y_i \partial y_j} T_{ij}\, d\vec{y}\, d\tau + \int_T\int_S \frac{\partial G}{\partial y_i} f_i\, d\vec{y}\, d\tau\right] \qquad (1)$$

Volume sources (quadrupole) — Surface sources (dipole)

The notation follows that of reference 1, where

G Green's function for geometry

f_i force of surface on fluid

T_{ij} Lighthill's stress tensor

Equation (1) is the starting point for the theories describing the simple surfaces on figure 1. The terms G, f_i, and T_{ij} are assumed to be known a priori from experimental measurement or analytical modeling.

For jet noise, the surface source term is neglected, the free space Green's function is used, and the stress tensor, T_{ij}, is approximated analytically. The noise generated by flow over a surface is more complex than jet noise in that both terms of equation (1) must be considered. In the following sections, available theory for specific surfaces is discussed.

Small chord airfoil. - Equation (1) is evaluated in reference 1 to determine the sound emission from a thin airfoil of small chord immersed in a finite turbulent flow (e.g. a jet). The free space Green's function is used, and one broadband noise source is assumed. This source is due to the random forces acting on the airfoil, which are caused by turbulent flow over the rigidly mounted stationary airfoil. If the airfoil is not rigid and stationary (non-moving with respect to the observer) there would be additional terms to consider. Quadrupole noise sources in the wake of the airfoil are assumed to be negligible. Pure tones are not included.

The airfoil chord is assumed to be small relative to the eddy size. This insures that the source is compact so that changes in retarded time can be neglected for all sound emission angles. The small chord assumption also insures that the mean flow and turbulence doesn't change as it flows past the airfoil. Linearity and a small spanwise correlation size permit the span of the airfoil to be broken down into a number of strip segments to account for three dimensional turbulence gusts. Any spanwise variations in the incident turbulence and velocity can be handled similarly.

Goldstein and Atasi (ref. 7) showed that this analysis applied only to a very thin airfoil. A finite thickness (or a finite angle of attack) will introduce changes in the mean flow that will change the spectra at high frequency. Only the fluctuating lift forces are included, which result from the transverse turbulence component. Any noise due to fluctuating drag forces is neglected.

Assumptions about the turbulence and flow are also made. The mean flow and transverse turbulence are assumed to be uniform along the span. The turbulence is assumed to be isotropic. The turbulence spectrum is also assumed to be adequately modeled by relationships given in reference 1. Finally, refraction, scattering and reflection, and shielding of the sound by any surrounding surfaces are also neglected.

After a lengthy derivation (see ref. 1), using the previous assumptions, an equation results which describes the three dimensional broadband sound emission. This relationship accounts for the effect of three dimensional turbulence gusts and compressibility. By limiting our interest herein to the sound field in the plane perpendicular to the airfoil ($\varphi = 0^\circ$) the equation is greatly simplified. This simplification results in equation (2), which describes the spectral intensity, l_ω, at $\varphi = 0^\circ$ as a function of the polar angle, θ_i

$$I_\omega(\theta_i, \varphi = 0^\circ) = \frac{3b\rho_o \overline{v^2}}{32} \left(\frac{c}{R}\right)^2 \frac{M_o^3 \sin^2\theta_i \sigma_1^4}{\alpha_o(\alpha_o^{-2} + \sigma_1^2)^{5/2}} \left| S_c(\sigma_1, M_o) \right|^2$$

where

$$\omega = 2\pi f, \quad \tau_o = \frac{2l_y}{c}, \quad M_o = \frac{V_i}{c_o} \quad \text{and} \quad \sigma_1 = \frac{\omega c}{2V_i} = \pi\left(\frac{fc}{V_i}\right) \tag{2}$$

The quantity $S_c\langle\sigma_1, M_o\rangle$ is the two dimensional compressible response function which is given by one of two functions that are described in reference 1. The function used depends on the value of the frequency parameter, f_M, which is given by

$$f_m = \frac{\pi fc}{c_o}\left(1 - M_o^2\right)^{-1} \tag{3}$$

When $f_M \geq 1$, the compressible response function is described by Fresnel integrals; when $f_M < 1$, Bessel functions are used. For small values of f_M the simple incompressible response function (i.e. Sears function) would also be applicable.

Equation (2) is converted to the 1/3 octave band sound pressure level, SPL, by accounting for the bandwidth and using an integrated value of I_ω over each 1/3 octave band, $\overline{I_\omega}$. The frequency will henceforth be the center frequency of the 1/3 octave bnads. The 1/3 octave band SPL can then be written as:

$$SPL = 10 \log_{10}\left\{\frac{2\pi}{\pi}(.2316)\left(\frac{V_i\sigma}{c}\right)\left(\frac{\rho_o c_o}{P_{ref}^2}\right)\overline{I_\omega}\right\} \tag{4}$$

Substitution of equation (2) into (4) results in the basic equation used in this report as follows:

$$SPL\langle\theta_i, \varphi = 0^o\rangle = 10 \log_{10}\left\{0.043 \underbrace{\left[\left(\frac{\rho_o c_o^2}{P_{ref}}\right)^2\left(\frac{bc}{R^2}\right)\left(\frac{V_i}{c_o}\right)^6\left(\frac{\overline{v^2}}{V_i^2}\right)\right]}_{F_1\left(T_o^{-3}, \frac{bc}{R^2}, V_i^6, \text{intensity}^2\right)} (\sin^2\theta_i) \underbrace{\left[\frac{\sigma_1^5}{\alpha_o(\alpha_o^{-2} + \sigma_1^2)^{5/2}}\left|S_c\langle\sigma_1, M_o\rangle\right|^2\right]}_{F_3\left(\sigma_1 = \frac{fc}{V_i},\ \alpha_o = \frac{l_y}{c},\ M_o = \frac{V_i}{c_o}\right)}\right\} \tag{5}$$

Amplitude — $F_2\langle\theta_i\rangle$ — Shape of spectrum

Shape of radiation pattern

Equation (5) can be broken down into three factors. The first factor, F_1, describes the amplitude of the sound at $\theta_i = 90^o$ in terms of the ambient temperature (T_o), span (b), chord (c), velocity (V_i) and turbulence

intensity. The second factor, F_2, describes the shape of the radiation pattern at $\varphi = 0^o$.

The shape of the spectrum is described by the third factor F_3. The amplitude of the sound is only slightly affected by F_3. It is a function of: the Strouhal number based on the chord length ($fc/V_1 = \sigma_1/\pi$), a Mach number ($M_o = V_1/c_o$), and the transverse turbulence scale length-to-chord ratio ($\alpha_o = l_y/c$). Measurements by Laurence (ref. 8) indicate that changes in the local mean velocity, V_1, do not cause either the local turbulence intensity, $\sqrt{\overline{v^2}}/V_1$, or scale length, l_y, to change noticeably. Therefore equation (5) indicates that the spectral shape is the same for each velocity (i.e. can be normalized by the Strouhal no.) except for the effect of compressibility at high frequency through the $M_o = V_1/c_o$ term. The intensity of the sound at a given angle θ_1 should therefore vary with velocity according to V_1^6.

The polar angle, θ_1, only affects the level of the sound, through the radiation pattern term, $\sin^2 \theta_1$. Therefore the spectral shape is independent of θ_1.

Equation (5) has no parameters describing the effect of the thickness or angle of attack of the airfoil. This means the experimentally measured sound emission, from airfoils of small but finite thickness, angle of attack and chord should not change over a range of these parameters, provided they are small enough for the theory to apply.

Equation (5) can also be used to closely predict the axisymmetric noise emission caused by a uniform turbulent flow passing over a small ring airfoil. Consider an airfoil (fig. 2(a)) that is rolled to form a hoop and located in the center of the mixing region of the jet (hoop diameter = nozzle diameter, d_n). According to reference 9, the span, b, in equation (5) should be replaced by half the circumference of the ring ($b = \pi d_n/2$ for the ring airfoil configuration shown as fig. 2(a)).

The flow impinging upon the straight airfoil described on figure 2(a) is not uniform as assumed by the theory. The theory indicates that the shape of the radiation pattern would not be affected by non-uniform flow. Calculations indicate that the relative level and the shape of the spectra would not be noticeably affected. However, the absolute level of the noise is affected, primarily through the turbulence intensity and mean velocity terms in F_1. As a consequence, the ring airfoil will be used to experimentally determine the absolute level of the noise.

Large chord airfoils. - With large chord airfoils and/or at high frequency or high Mach numbers, the quantity $f_M = \pi fc/c_o (1 - M_o^2)^{-1}$ becomes large. When $f_M \geq 1$ the time for an acoustic disturbance to traverse the chord of the airfoil becomes too long, compared to the period of oscillation, for the process to be considered to be incompressible. Therefore the incompressible response (Sears) function should completely fail to predict the sound from large chord airfoils, especially at high frequency. In such a flow, the fluctuating lift noise source should move toward the leading edge as f_M increases. In other words, the trailing edge region of a very long chord airfoil should contribute very little to the noise emission at high frequency. In fact, at high frequency the fluctuating lift acting on an infinite chord airfoil should be the same as for a small chord airfoil. Therefore the high frequency part of the spectra for airfoils of different chord lengths should be about the same.

For large chord airfoils chordwise variations in retarded time are not negligible, therefore small chord theory (equation (5)) does not apply to all angles. However, because the noise emission at $\theta_1 = 90^\circ$ is not affected by variations in retarded time, equation (5) should be able to predict the spectra at $\theta_1 = 90^\circ$ for airfoils of any chord.

The shape of the radiation pattern is predicted from another applicable theoretical development, described in reference 1 by $V_1^5 \sin^2(\theta_1/2)$, providing the source region is very close to the leading edge compared to the wavelength of the sound. Therefore this latter radiation pattern would tend to be more accurate at high frequency. Equation (5) also indicates that the sound intensity should change as V_1^5 for a large chord airfoil at $\theta_1 = 90^\circ$. The reason for this is that for large chord values the $|S_c(\sigma_1, M_o)|^2$ term becomes proportional to $1/V_1$.

For large values of f_M two additional characteristics may appear. First, the quadrupole term (eq. 1) may no longer be negligible. Therefore at angles close to the jet we may see higher velocity power laws at high frequency. Also, the noise sources may become less compact.

Cylinders. - The noise from very small cylinders, which produce tones (aeolian tones), is also described in reference 1. For small cylinders (i.e. low Reynolds numbers) there is a periodic shedding of vortices which causes a fluctuating lift force on the cylinder. This generates a tone of the same frequency. According to experiments by Phillips (ref. 10), for Reynolds numbers of up to 200, the Strouhal number of the tone is 0.18. Turbulence measurements (ref. 11) indicate that this periodic eddy shedding of vortices persists up to a Reynolds number of about 10^4. At higher Reynolds numbers the wake becomes turbulent. This would result in random fluctuating forces and broadband noise. Theory indicates the radiation pattern should be $\sin^2 \theta_1$ for all cases.

For thick bodies such as cylinders there is also the possibility of source non-compactness, thickness effects or a fluctuating drag force noise. But for thin bodies such as airfoils these effects should be negiligible compared to the noise caused by fluctuating lift forces. These effects would tend to become apparent in experimental data as $\varphi \to 90^\circ$ because fluctuating lift noise goes to zero.

APPARATUS

Test rig. - Two similar test rigs of different size were used to obtain the noise data in this paper. Each system conceptually looked like the small rig shown in figure 3. The small rig consisted of the following (proceeding downstream): a 10 cm flow control valve; a valve noise quieting section; a long straight run of 10 cm pipe; and finally a 7.6 cm diameter perforated plate nozzle (4 cm equivalent diameter). The first valve noise quieting element was a perforated plate. Downstream of that was a large volume no-line-of-sight muffler. The larger rig used larger but similar flow hardware and a 10 cm circular nozzle. None of the nozzle jet noise data reported herein were affected by internal valve noise, either through the nozzle exit or by direct radiation through the pipe.

The nozzles used are shown on figure 2. These arrangements and subsonic flows were used in order to avoid feedback tones. As will be shown, weak feedback tones still affected a few 1/3 octave bands of some of the high velocity data taken with the circular nozzle. Only a small correction was needed to remove this contamination. The test airfoils were rigidly mounted to the nozzle inlet pipe. The turbulent airstream from the two types of nozzles (fig. 2) was impinged upon the test airfoils in free space with no enclosing duct.

Surface geometries tested. - The surfaces tested, airfoils and cylinders of varied size and cross section, are shown on figure 4 and table 1. Most of the experiments involved straight span airfoils or cylinders where the impinging flow is non-uniform. Uniform impinging flow was achieved with a ring airfoil (fig. 2). The airfoil chord length, thickness and angle of attack were varied.

Acoustic instrumentation and data analysis. - The noise data were measured outdoors with either of two types of semicircular microphone arrays that were centered on the nozzle exit. All of the results reported were corrected (less than 1 dB and 5°) to an effective center at the leading edge of the airfoil. Condenser microphones (1.27 cm) with windscreens were used. Each array had a microphone radius of about 50 nozzle diameters to assure that they were well into the far field for jet noise. The data were taken either with a horizontal or vertical (shown in fig. 3) semicircular microphone array, with open cell acoustical foam on the ground. Either array resulted in free field noise data for frequencies above 200 Hz. Background noise had an effect upon the data below about 400 Hz, but only when the low frequency sound level was low.

The data were measured by 11 microphones on a semicircle of 3 or 4.6 meter radius from $\theta_i = 20^\circ$ to 160°. In all arrays, the polar angle $\theta_i = 0^\circ$ corresponds to the nozzle inlet. The test surface was generally rotated at the flange about the nozzle centerline in order to vary the azimuth angle φ without changing the flow condition. At an azimuth angle of $\varphi = 0$ the test surface is perpendicular to the microphone plane (e.g. vertical microphone array of fig. 3). At $\varphi = 90^\circ$ the test surface would be in the plane of the microphones. Measurements showed that the foam covered support was low enough so it did not affect the noise radiated at any azimuth angle reported.

The frequency range of the data was 50 Hz to 20 kHz. The noise data were analyzed directly by an automated one-third-octave band spectrum analyzer; some data were also tape recorded for subsequent narrowband analysis. Both methods yielded sound pressure level spectra (SPL) referenced to 2×10^{-5} N/m^2. The one-third-octave band SPL spectra reported were corrected (by ARP 866)[1] for atmospheric attenuation (less than 2 dB at 20 kHz) so that the reported data are lossless. The small contribution of background noise was also removed.

The jet noise, which was separately measured with the support in place, was also removed. Therefore the 1/3 octave data reported (SPL_c) represents the noise from the test surface alone. The SPL_c data reported required no more than a 2 dB correction for jet noise; usually the correction

[1] In this case this correction is numerically equivalent (within 1/2 dB) to the corrections of the new proposed ANSI standard.

was nearly zero. Those data points where the SPL is 2-4 dB above the jet noise are noted with a hash mark. These corrected data were summed spectrally to produce the overall sound pressure level, $OASPL_c$. The data measured in a given φ-plane were summed spatially to produce an effective power spectrum, PWL_b, (see ref. 12). The reported narrowband spectra SPL, were not corrected for the small contributions of atmospheric attenuation, background noise or jet noise.

Considering the microphone calibrations, periodic checks on the data system, and the data averaging, it was determined that each one-third-octave band sound pressure level was repeatable from day-to-day to within about ±1 dB. Jet noise spectra measured with this facility are overall within 1/2 dB of previously published jet noise data.

RESULTS AND DISCUSSION

Small Chord Airfoils

Noise contours. - The total sound emission from a small chord airfoil is shown in figure 5. The data taken on a 4.6 m radius circle in the $\varphi = 0^\circ$ azimuthal plane. This airfoil, which will be considered to be the nominal small airfoil, had a 2.5 cm chord length and a thickness of 0.32 cm. It was immersed in the turbulent airstream of the jet of the circular nozzle (see fig. 2(a)). The peak impingement velocity, V_{ip}, was 94 m/sec. Figure 5 is an iso-noise contour plot made up of curves of constant sound pressure level, SPL_c. This figure is a useful introduction to the acoustic data for the small chord airfoil that is to be shown on the next several plots. From this plot it can be seen that the maximum level occurs at around 2.5 kHz and near $\theta_i = 90^\circ$. The peak region is fairly flat with steep slopes at high and low frequency. The dashed line is the locus of spectrum peaks at each θ_i. This curve shows that the frequency of the peak level is almost independent of θ_i. For a fixed frequency the level falls off about 5 dB at $\pm 60^\circ$ from 90°. The contour shape for $\theta_i < 90^\circ$ is approximately elliptical and symmetrical about the peak locus. The theory indicates that this shape should also occur at $\theta_i > 90^\circ$. The steeper drop off at $\theta_i > 130^\circ$ and high frequency is probably due to refraction of the airfoil noise by the jet shear layer. The higher SPL_c level at low frequency and $\theta_i > 130^\circ$ is probably due to an additional noise source.

The complete noise emission data for each airfoil configuration will be broken down (as indicated by equation (5)) into the shape of the spectra, shape of the radiation pattern, and the amplitude. This breakdown permits a more accurate comparison of the theory with the data. These comparisons will help determine shortcomings in the theories, and determine the range of parameters and geometrical variations where a theory applies.

Radiation pattern at several frequencies. - Sound pressure level data, SPL_c, at several constant frequencies are plotted as a function of polar angle on figure 6. The curves are separated in level in order to avoid overlap. The theory (eq. (5)) indicates that the shape of the radiation pattern at all frequencies should be described by $\sin^2 \theta_i$. But refraction

of the airfoil noise emission by the jet shear layer should decrease the level below $\sin^2 \theta_i$ at large θ_i and at high frequency. A recent theory by Goldstein (refs. 13 and 14) indicates that there may be a modification of the radiation pattern at low frequency that results in additional noise at large θ_i. The purpose of this plot is to compare the measured shape of the SPL_c radiation pattern to the theory. As such the level of the $\sin^2 \theta_i$ curves are adjusted for the best overall fit of the data where the theory is expected to apply. The data at a frequency of 2.5 kHz, which is near the peak level, closely follows the theoretical $\sin^2 \theta_i$ curve everywhere.

At higher frequency the data fall below the $\sin^2 \theta_i$ curve for $\theta_i > 130^\circ$. This is probably due to the refraction of the airfoil generated noise by the jet shear layer; refraction is not included in the theory. Any data that is affected by refraction will not be used for comparisons to the theory.

At low frequency (800 Hz) there apparently is additional noise, above the $\sin^2 \theta_i$ level, for $\theta_i > 100^\circ$. This additional noise is not due to residual jet noise that was not completely removed in obtaining the SPL_c, because all the SPL data at 800 Hz were at least 7 dB above the jet noise. Goldstein (ref. 14) indicates that there is a modification in the radiation pattern at low frequency that results in additional noise near the exhaust for a quadrupole source (e.g. jet noise) and also for a dipole source (e.g. surface noise). This theory accurately explained low frequency jet noise data (refs. 13 and 14). Therefore, it seems reasonable to assume it will also work well for the low frequency noise from a small chord airfoil which has a dipole source. The shape of the radiation pattern that includes this additional noise is described by the more complex second equation on figure 6. This equation was derived in reference 14. The radiation pattern resulting from this equation is also shown in figure 6 along with the $\sin^2 \theta_i$ radiation pattern. The relative levels of these two radiation patterns and the value of the coefficient (2/3) were selected so that the logarithmic sum of the two patterns matched the data. The data appears to show a gradual transition from the $\sin^2 \theta_i$ pattern to the second equation as the frequency decreases. In any event, this additional noise at low frequency can probably be ignored for most practical applications.

Shape of spectra. - The theory (eq. (5)) indicates that the shape of the spectra is not a function of polar angle. Figure 7 contains plots of the spectra that were measured at several polar angles, θ_i. The data are for the nominal 2.5 cm chord airfoil at three peak impingement velocities. The SPL_c data plotted have been normalized to the $OASPL_c$ so that the collapsed data will clearly show the shape of the spectra. The spectral shape does not change systematically with θ_i for the large range of $\theta_i (35^\circ < \theta_i < 130^\circ)$. Refraction affects the spectral shape for $\theta_i > 130^\circ$. Therefore, the theoretical characteristic of unchanging spectral shape is verified by the data up to 130°, where the experiment satisfies the requirements of the theory. The difference between the $OASPL_c$ and the peak of the SPL_c spectrum is about 9-1/2 dB for all velocities.

According to equation (5) the shape of the spectra is only a weak function of velocity. Indeed, the data and theory both indicate that the shape of the spectra at low velocity is only slightly less peaked than at high velocity.

The shapes of the spectra in figure 7 were calculated from equation (5) for this airfoil. The turbulence scale length and impingement velocity were evaluated at the position of the airfoil from turbulence data measured by Laurence (ref. 8) in the jet of a circular nozzle. The local velocity, V_i, of the theory was taken to be the peak impingement velocity across the span of the airfoil, V_{ip}. The theory assumed isotropic turbulence while measurements (ref. 8) show that the axial length scale is twice as large as the transverse. Therefore the scale length could be anywhere between these limits. The value of the scale length used in the calculation ($\ell_y = 1.9$ cm) is 20 percent larger than the value for ℓ_y/d_n reported in reference 8. The magnitude of the length scale will be discussed further in a subsequent section.

The solid curve is the result from equation (5) using the two dimensional compressible response function for $S_c(\sigma_1, M_o)$, while the dashed curve is obtained by using the incompressible Sears function to evaluate $S_c(\sigma_1, M_o)$. The shapes of the spectra from the compressible solution agree quite well with the data. The incompressible solution does not agree at high frequency. The high frequency part ($f_m \geq 1$) of the compressible response function solution applies for frequencies above the X noted on the curves. The incompressible solution closely agrees with the more complex Bessel function solution used for $f_m < 1$. Apparently the Bessel function solution can be replaced by the qually accurate but simpler incompressible solution where $f_m < 1$. But for $f_m > 1$ the incompressible solution fails to match the data.

Although the agreement at high frequency between the compressible theory and the data is quite good, the theoretical result has one feature not seen in the data. At about 20 kHz the spectra flattens out. This is due to the Fresnel integral terms in the high frequency part compressible response function, which slowly oscillates with frequency. This will be discussed further in a later section.

The theory requires no flow separation off the airfoil. It also requires that the flow near the airfoil is uniform in the chordwise direction and adequately described by the turbulence spectra used in reference 1. Measurements by Boldman (ref. 15), at several locations near the 2.5 cm chord straight span airfoils used herein, indicated that these requirements were satisfied.

At the peak of the spectrum for the highest velocity shown on figure 7 there were some tones in the data that were removed because they were not considered by the theory. Figure 8 contains narrowband spectra at $\theta_i = 100^o$ for a group of impingement velocities. Tones occur primarily in the 1.6 kHz 1/3 octave band of the data taken at a velocity of 132 m/sec. In this worst case, the change in the SPL_c that resulted from the removal of the tones was 3 dB. The tones were much weaker at higher and lower velocities and in the adjacent 1/3 octave bands. The frequency of the strong tone did not change with angle, and the level of the tone followed the same relationship as the broadband noise ($\sin^2 \theta_i$). Therefore, the correction needed to re-

move the tone was constant for all angles. The same result occurred for airfoils with different chords that were at the same leading edge location.

Overall radiation pattern. - The radiation pattern of overall noise is plotted on figure 9 for several peak impingement velocities, V_{jp}. The theoretical radiation pattern shape, $\sin^2 \theta_1$ fits the data at all velocities quite well. Recall from figure 7 that refraction only affected the data at high frequencies. The SPL_c radiation pattern at the frequency of the peak noise followed $\sin^2 \theta_1$. Therefore it is not surprising that the $OASPL_c$ pattern, which is dominated by the unaffected peak SPL_c, is described by this pattern. The change in the $OASPL_c$ with velocity is described at all θ_1 by the velocity power law of the theory, V_j^8.

Effect of non-uniform flow impingement. - The straight span airfoil crosses the jet (see fig. 3(a)) at the center of the mixing region. As a consequence there are radial and therefore spanwise velocity and turbulence gradients. The theory (eq. (5)) assumes the flow is uniform along the span. Since the straight span airfoil has a non-uniform impinging flow the measured absolute level of the noise cannot be directly compared to the theory. However, accurate experiments to determine the effect of changes in geometry or velocity on the relative noise level can be performed. Accurate experiments to measure the shape of the radiation pattern and the shape of the spectra can also be performed. The straight airfoil was moved radially ±1 cm from the nominal position at the center of the mixing region at a fixed jet velocity. The level varied about ±2 dB but the shapes of the spectra and radiation pattern were unchanged from those shown on figures 7 and 9.

Ring airfoil. - A ring airfoil was used (see fig. 2(a)) to experimentally verify the theoretical prediction for the absolute level because the velocity and turbulence impinging on this asixymmetric airfoil are uniform. The location and cross section of the airfoil was the same as for the straight span airfoil (see fig. 2(a)).

From the theory, it can be expected that the noise emission from the ring airfoil should be very close to the straight span airfoil, except for the absolute level. The shape of the $OASPL_c$ radiation pattern for the ring airfoil (data not shown) was exactly the same as for the straight span airfoil. The shape of the spectra for the ring airfoil is compared at $\theta_1 = 90^\circ$ to that for the straight airfoil on figure 10. Here too there is no significant difference. The theoretical spectra and relative level are compared to the data at 90° at three velocities. The agreement is excellent.

Absolute level. - The prediction of the absolute level of the noise was checked with the ring airfoil. This was the only geometry tested that has a uniform impinging flow along the span as required by the theory. The ring airfoil was located at the center of the mixing region where all quantities required by equation (5) are known from reference 8. Based on the ring airfoil theory discussion, the span, b, is replaced by half the circumference of the ring. The measured $OASPL_c$ is compared to the calculated level on figure 11 for the conditions listed on the figure. The excellent agreement of the absolute levels is particularly significant since no empirical adjustments have been applied to the theory.

Up to this point it has been shown that the basic theory for a small chord thin airfoil accurately predicts the total noise emission. The experimental limitations proved to be small or of no consequence. The

next task is to determine how small the airfoil thickness and chord must be in order to satisfy the assumptions of the theory.

Effect of thickness. - Reference 7 indicates that the high frequency region of the spectra should be affected by finite thickness. A thick airfoil distorts the mean flow, which would affect the spectra above some frequency. The spectra from two straight span airfoils of different thickness are compared on figure 12. The nominal airfoil (thickness, 0.32 cm and chord length, 2.5 cm) was compared to an airfoil of 1 cm thickness and the same chord length at the same peak impingement velocities, V_{ip}. The spectra differ only at high frequency, with the thick airfoil being quieter, especially at low velocity. The spectra for the thick airfoil deviates from the thin airfoil data and the theory, at a thickness to wavelength ratio of about 0.1. The shape of the $OASPL_c$ radiation pattern for the thick airfoil is the same as that for the thinner nominal airfoil. Practical airfoils are typically thicker than the nominal airfoil, therefore thick airfoil theory may have to be used in practice.

Effect of Chord Length

The sound emission at $\theta_i = 90^\circ$ is not affected by variations in retarded time. Therefore, equation (5) should be able to predict the spectrum and noise level at 90° for an airfoil of any chord length. But there is no theory spelled out in reference 1 to predict the spectra at other angles[2]. There is a different theory described in reference 1 to predict the radiation pattern for an infinite chord airfoil, where the source region is very close to the leading edge relative to the wavelength of the noise.

Overall radiation pattern. - Straight span airfoils of varied chord length were run at the same leading edge position, as shown on figure 2(a). This insured that the impingement velocities were the same for all chords. All the airfoils had the same thickness, 0.32 cm, and the same leading and trailing edge shape (see fig. 4a-2). The length of the straight part of the airfoil was extended in order to vary the chord from 1 cm to 240 cm.

The radiation pattern of the overall noise from these airfoils, at an impingement velocity of 94 m/sec, is plotted on figure 13. The 2.5 cm chord airfoil is the nominal small chord airfoil used for figures 5 through 9. The radiation pattern for the 1 cm and 2.5 cm chord airfoils are both described by the theoretical pattern, $\sin^2 \theta_i$. However the pattern for the 10 cm chord airfoil is clearly not described by $\sin^2 \theta_i$. Therefore, so far as the pattern is concerned the 1 and 2.5 cm chord airfoils are short enough to be considered to be short chord airfoils; the 10 cm chord is too long. In other words, the small airfoil theory (eq. (5)) is applicable at all θ_i when the transverse turbulence scale length is larger than 75 percent of the chord.

As the chord increases there is a gradual increase in the sound level at large θ_i, relative to the $\sin^2 \theta_i$ pattern shape. Eventually

---

[2]A theory accounting for variations in retarded time that should treat other angles has been recently published (ref. 17).

the infinite chord case is reached. The theoretical radiation pattern for the infinite chord airfoil, $\sin^2(\theta_1/2)$, describes the shape of that data fairly well. The change in the level at $\theta_1 = 90^\circ$ with chord length was calculated from the theory, and the applicable theoretical pattern was put through those points (X on fig. 13). The relative theoretical levels agree well with the data.

Spectra at 90°. - The spectra measured at $\theta_1 = 90^\circ$ for these varied chord airfoils is plotted on figure 14(a). Notice that the low frequency part of the spectrum moved to lower frequency as the chord increased. The high frequency part of the spectrum was essentially unchanged as the chord increased because at high frequency fluctuating lift is independent of chord. As the chord increased the spectra becomes less smooth at low frequency. The shape of the spectra for the 1 cm chord is exactly the same as for the nominal 2.5 cm chord airfoil. Since there was no change in shape, the nominal chord length is clearly small enough to satisfy the requirements of the small chord airfoil theory. The 1 cm chord airfoil was not taken as the nominal small airfoil because the spectral range of the useful SPL_c data is smaller.

The spectra can be predicted by equation (5) at $\theta_1 = 90^\circ$. Figure 14(b) contains the predicted spectra for the chord lengths involved in figure 14(a). The overall trends in the analytical results are clearly the same as the data. The transverse turbulence scale length ($l_y = 1.9$ cm) used in figures 7 and 10 for the 2.5 cm chord length was also used in this calculation. If the scale length were allowed to increase with chord length, the agreement with the data would be much better for all chord lengths.

The velocity of the jet flow along these airfoils did not noticeably decay for the 10 cm long or shorter chord airfoils. The peak velocity decayed about 16 percent for the 61 cm chord airfoil. For the 240 cm chord thsignificant noise is generated at the trailing edge because the decay was 60 percent. Theory indicates that the source remains near the leading edge as the chord increases. Therefore the fact that there is decay is not inconsistent with the assumptions of the theory; it simply permits a very large but finite chord to be considered to be infinite except for small f.

The following are a few points of interest about the theoretical results. The X symbols on the curves are where $f_m = 1$. For higher frequencies than indicated by the X, the high frequency compressible solution with Fresnel integrals must be used; for lower frequencies, the simple incompressible solution is just as accurate as the low frequency compressible solution. The dips and peaks, which occur in the high frequency compressible solution region, are due to oscillations in the Fresnel integral terms. The data for the large chord airfoils also show this characteristic, but the frequencies of the dips and peaks do not quite agree. Because of Fresnel integral oscillations, there may be a difference between calculating the SPL at the center frequency of the band or calculating an average value over the 1/3 octave band as done herein. The simple calculation caused an error of no more than 1 dB at a few frequencies.

The "Noise Component Method" (e.g. refs. 9, 15, 18, and 19) uses the analytical descriptions of the noise from the simple surfaces shown in figure 1. These are added together as independent noise sources with

empirical coefficients in order to describe the noise from complex surfaces. The small and infinite chord airfoils are two such components. But the results just presented showed a gradual transition as the chord increased. The analytical model, developed for the small chord airfoil, can also be used to describe the spectra at 90° for all chord lengths. This model has a lift fluctuation between the semi-infinite to the infinite board as $L_e \rightarrow \infty$ (see fig. 1(c)). This discussion does not invalidate the very useful Noise Component Method but rather it suggests some modifications are needed.

Infinite chord airfoil. - The 245 cm chord airfoil is considered to be essentially infinite for the following two reasons. The theoretical curves for chord lengths of 61 and 245 cm indicate that the noise is no longer changing significantly with chord length. Secondly, the velocity coming off the trailing edge was so low that any noise generated there could be neglected.

Spectra at several angles for the 245 cm chord airfoil are plotted on figure 15(a) for an impingement velocity of 94 m/sec. As θ_i increases the spectra become very much more peaked. Notice also that these free field spectra are not even approximately smooth.

Figure 15(b) contains the SPL_c radiation pattern at a number of frequencies. The peak noise occurs near 630 Hz. The theoretical radiation pattern at a constant frequency is described by $\sin^2(\theta_i/2)$. This theoretical relationship describes the data on figure 15(b) at high frequency, where the source would tend to be close to the leading edge. This pattern does not accurately describe the data at low frequency (e.g. 630 Hz, where the peak noise occurs). At high frequency there is evidence of some refraction by the jet shear layer.

The overall radiation pattern, $OASPL_c(\theta_i)$, is plotted on figure 16(a) for several velocities. The theoretical pattern, $\sin^2(\theta_i/2)$, fits the low velocity data quite well. But as the velocity increases the discrepancy becomes more pronounced, due to the peaked spectra. Notice that the velocity power law of the data is $V_i^{5.5}$ for $\theta_i < 120°$, and about V_i^6 for larger θ_i. Theory indicates the $OASPL_c$ power law should be V_i^5.

Sound pressure level spectra at 90° are plotted on figure 16(b). These are for the infinite chord airfoil at several velocities. The theoretical spectra and relative levels closely agree with the data. In order to achieve this agreement a transverse scale length of $\ell_y = 3.2$ cm was used. In figure 14(b) a value of $\ell_y = 1.9$ cm was used for all chord lengths but the agreement at low frequency needed improvement. If a scale length that increases with chord length had been used for figure 14(b), the agreement would have been improved for all chord lengths. The compressible solution was used for figure 16(b). The incompressible solution was not used because it failed completely.

On a constant Strouhal number basis the theory predicted a change in level described by a $V_{ip}^{5.5}$ power law at all frequencies. But as shown on figure 16(b) the data indicate the power law is higher at high frequency. At angles closer to the exhaust axis (e.g. $\theta_i > 120°$) the power law at

all frequencies is V_{jp}^7. As mentioned in the analysis section, this may be because the quadrupole term of equation (1) is no longer negligible.

Supplementary Experiments

Most of the experiments that follow were performed with the perforated plate nozzle (fig. 3(b)). The airstream from this nozzle was turbulent and straight span surfaces were mounted across the jet on the nozzle centerline. The leading edge of the test airfoils and cylinders were all placed 7.6 cm downstream of the nozzle. Measurements had been made of the axial turbulence and velocity at this position (ref. 15). The flow was not uniform. The shape of the turbulence spectra was about the same as for the circular nozzle experiment and the length scale was about 1/3 as large. Since the transverse turbulence was not measured the acoustic data can only be used to show changes in the noise level and spectra caused by changes in surface geometry at fixed velocity. And the shape of the radiation pattern can be compared to theory.

Separation of airfoil noise sources. - Experiments were run to separate the noise generated in several areas of a large chord airfoil. This was done by using a very long chord airfoil to eliminate trailing edge noise, and airfoils with no leading edge to eliminate that source. A very long plate with no leading edge can only generate noise from the boundary layer flow over the surface.

The PWL'_c measured for these geometries at the same velocity is plotted on figure 17(a). All airfoils were smooth and of the same thickness (1 cm) and shape. The peak velocity at $x = 7.6$ cm was 115 m/sec. The effective power spectra level at $\varphi = 0^o$, PWL'_c, was used for this comparison because the polar distribution of the noise varies with the chord length.

Surface 1 used a very long chord airfoil (245 cm long). The rounded leading edge was removed and sealed against the perforated plate (fig. 4(a-4)) such that there could be no leading edge noise. The only noise source left was the turbulent boundary layer flow over the long airfoil surface. The resulting noise, as indicated in figure 17(a) was buried somewhere in the jet noise, and well below the levels for the other sources. Boundary layer noise (BL) can be effectively neglected in the subsequent comparisons in figure 17.

For surface 2 the rounded leading edge was installed and moved to a position 7.6 cm downstream from the nozzle. This surface should only have leading edge (LE) noise. The spectrum is strictly high frequency noise. This result is expected since the theory indicates the source is near the leading edge where the velocity is the highest and the turbulence scale the smallest. The overall radiation pattern, $OASPL_c(\theta_i)$, is shown on figure 17(b). The maximum level occurs in the infinite direction of the plate, which is consistent with the theory.

Surface 3 has no leading edge and the plate has been shortened to 45 cm so that the velocity at the trailing is relatively high. Therefore this configuration only generates trailing edge (TE) noise and

the spectrum (fig. 17(a)) contains mostly low frequency noise. This result is simply explained relative to surface 2. At the trailing edge source location the turbulence scale is larger, due to the boundary layer flow, and the velocity is lower. The theoretical pattern for an infinite plate would peak in the infinite direction of the plate (i.e., small θ_i). The pattern for surface 3, which is not as long as surface 2, approaches that result.

Surface 4 has both leading and trailing edge noise sources. The leading and trailing edges are well separated so that these sources can be considered to be independent. The leading edge and trailing edge velocities that were measured indicated they were the same as those for surfaces 2 and 3 respectively. The leading edge noise of surface 2 and the independent trailing edge noise of surface 3 should add up to equal the noise measured for surface 4. The spectra and radiation pattern data plotted on figures 17(a) and 17(b) show that this is indeed the case. The same results and trends occurred for data taken at higher velocities.

Surface 5 is an airfoil with a smaller chord. The leading and trailing edges are too close for the sources there to be considered to be independent. Nevertheless a comparison of results is of qualitative value. The leading edge source would be essentially the same as before, but because the chord is small, the trailing edge source is now affected by a higher velocity and smaller turbulence scale length. Therefore the trailing edge region would be expected to generate high frequency noise, roughly equivalent to the leading edge noise. Figure 17(a) indicates that this description is reasonable. The airfoil used was the thick airfoil that was used with the circular nozzle (fig. 12). The turbulence scale length is smaller here than it was with the circular nozzle. Therefore the 2.5 cm chord airfoil can no longer be considered to be small as it was with the circular nozzle. Consequently it is not surprising that the radiation pattern for this surface (surface 5) is not described by the theoretical pattern for the small chord airfoil ($\sin^2 \theta_i$).

Other effects. - Noise data were also obtained for the 1 cm thick, 2.5 cm chord airfoil in two azimuthal planes ($\varphi = 0^\circ$ and $\varphi = 80^\circ$) in order to look for other effects beside fluctuating lift noise. These data are shown in figure 18. In the formulation of the theory for a thin small chord airfoil, any noise caused by thickness, non-compactness, and fluctuating drag was neglected. The fluctuating lift radiation pattern for the overall noise is given by $\sin^2 \theta_i$. At increased values of φ the $\sin^2 \theta_i$ pattern shape will decrease in level uniformly, approximately according to $\cos^2 \varphi$. At $\varphi = 80^\circ$ the $\sin^2 \theta_i$ pattern will decrease 15 dB if there is no drag dipole, source non-compactness or thickness effects. The l_y/c ratio for this airfoil is too small to have the $\sin^2 \theta_i$ pattern of a small airfoil. Nevertheless it is clear from figure 18 that the pattern at $\varphi = 0^\circ$ dropped 15 dB almost uniformly. Therefore these other effects are apparently very weak even for this relatively thick airfoil. There was also no evidence of these other effects with the thick and thin, small or infinite chord airfoils tested previously (e.g. figs. 13 or 17). On the other hand a strong drag dipole was observed at $\varphi = 90^\circ$ for the airfoil used in experiments reported in reference 20.

Effect of angle of attack. - There is no angle of attack term in equation (5). The effective power spectrum for an 8.9 cm chord unsymmetrical airfoil is shown on figure 19 for several angles of attack. The noise did not increase at 10°; and increased by no more than 1 dB until the angle of attack increased beyond 20°. Consequently, equation (5) is valid up to a 10° angle of attack. At an angle of attack of 40° there was large scale flow separation. The radiation pattern of the overall noise in the $\varphi = 0°$ plane increased 1 dB uniformly at each angle in going from a 0° to 20° angle of attack. The same insensitivity occurred with the nominal small airfoil at a 10° angle of attack (i.e. the results were the same as for fig. 7).

Effect of roughness and shape. - A series of long chord airfoils (45 cm chord length) were placed 7.6 cm downstream of the perforated plate nozzle. The noise emission from each was compared at the same peak impingement velocity, V_{ip}. These geometries, which are shown on figure 20, are similar to engine exhaust duct acoustic splitters. Configuration A is the same as surface 4 in figure 17. This reference surface has high frequency leading edge noise and low frequency trailing edge noise. The group of A configurations will show the effect of surface roughness on the noise generation. The flat surface roughness is varied from smooth to rough without changing the dimensions of the airfoil. The smooth surface (configuration A) was first replaced by an 8 percent perforated plate glued to a solid wood core (configuration A-1). The noise remained unchanged. Then a coarse perforated plate was substituted (configuration A-2). There was a 2 dB reduction in the noise at low frequency. Apparently the boundary layer flow over this rough boundary affected the trailing edge noise (low frequency) generation. The trailing edge of the smooth airfoil (A) was removed, resulting in configuration B. The noise was reduced close to 4 dB at low frequency because the trailing edge noise generation was affected. A thick airfoil, airfoil C (2.5 cm thick), was also substituted for airfoil A (1 cm thick); the noise was reduced about 4 dB for the same reason. There was additional tone-like noise at 12.5 kHz for the A-2 surface; the Strouhal number of the tone was about 0.2 based on the diameter of the holes.

Circular cylinders. - Circular cylinders of varied diameter, d, were run at a constant peak impingement velocity, V_{ip}, of 172 m/sec. The leading edge for all cylinders was 7.6 cm downstream from the nozzle, as shown in the sketch on figure 21. The diameter of the cylinders ranged from 0.31 cm to 6.2 cm, corresponding to a Reynolds number range of 1.6×10^4 to 2.5×10^5. The effective power spectra at $\varphi = 0°$, PWL_c, for these cylinders is plotted on figure 21(a). The shape of the spectra varied from tone-like for the 0.31 cm and 0.63 cm diameter cylinders to broadband for the 2.5 cm and 5.2 cm cylinders. Narrowband spectra, taken for the 0.63 cm and 2.5 cm cylinders, further verified this observation. The Strouhal number (see table on fig. 21(a)) was 0.18 for the small cylinders with the relatively narrowband spectra (Reynolds number $\leq 5 \times 10^4$). The Strouhal number increased for larger cylinders indicating that diameter was no longer the proper characteristic size. Turbulence measurements in the wake of cylinders were described in reference 16. The same type of spectra transition and Strouhal number were noted in the turbulence data at these Reynolds numbers. Apparently the eddies in the wake of the small cylinders are highly correlated, producing a periodic lift force and therefore periodic noise

(aeolian tones). When the diameter was large the flow structure in the wake becomes more random and the noise produced was broadband.

The shape of the $OASPL_c$ radiation pattern for all these cylinders did not change with velocity, and the noise followed a V_j^6 power law. The smallest cylinder (0.31 cm diameter) produced very high frequency noise, which was noticeably refracted near the exhaust. The $OASPL_c$ radiation pattern for the other cylinders was not affected. The shape of the radiation pattern was the same for the 0.63, 1.28 and 2.5 cm diameter cylinders. These cylinders had the fluctuating lift radiation pattern ($\sin^2 \theta_i$) at $\varphi = 0^\circ$ as shown on figure 21(b). A similar experiment was performed with a 2.5 cm diameter cylinder formed as a ring (10 cm diameter toroid downstream of the 10 cm circular nozzle). These results were also described by a $\sin^2 \theta_i$ pattern. On the other hand the largest cylinder (5.2 cm diameter) had a pattern that was more like a large chord airfoil (i.e. peak between $\theta_i = 120^\circ$ and 160°). Perhaps at that diameter the source is no longer compact, or thickness effects have become strong.

Figure 21(b) also contains the radiation pattern for the 0.63 and 2.5 cm cylinders at $\varphi = 85^\circ$. The $\sin^2 \theta_i$ pattern that applies at $\varphi = 0^\circ$ did not uniformly drop 21 dB in level as required by theory (approximately $\cos^2 \varphi$). Therefore, additional effects, such as source non-compactness, thickness effects and/or a drag dipole source should be considered.

Effect of cross sectional shape. - The PWL'_c spectra at $\varphi = 0^\circ$ for a number of cylinders of varied cross section are compared on figure 22. These are compared at the same impingement position, velocity, and thickness. The bodies with the blunt trailing edges are the quietest overall. The three bodies with flow separation have comparable noise levels at high frequency, where the airfoil is quieter.

SUMMARY

The following summarizes the acoustic results of a comparison of theories and experimental data concerned with surfaces immersed in turbulent flow from a jet:

1. The experimental apparatus produced acoustic data that permitted an accurate comparison with available small airfoil analyses over a large spatial (θ_i, φ) and spectral range, for a range of parameters, including: flow, chord length, thickness, angle of attack and shape.

2. Small airfoil theory (compressible) accurately predicts the complete noise emission (absolute level, spectra, and radiation pattern) provided:

(a) the transverse turbulence scale length is larger than about 75 percent of the chord length,

(b) the angle of attack is less than about 10°, and

(c) the airfoil thickness to wavelength ratio is less than about 0.1.

3. This theory also accurately predicts the relative level and spectra for large chord airfoils at $\theta_i = 90^\circ$, $\varphi = 0^\circ$.

4. The shape of the $OASPL_c$ pattern for the infinite chord airfoil is adequately predicted by another theory, except at the location of the peak noise for high velocity.

5. The noise sources at the leading edge, trailing edge and in the boundary layer flow of a long chord airfoil were approximately separated in a single experiment. The trends in the data were in agreement with the theory.

6. Source non-compactness, thickness effects, or a drag dipole are evident in the data taken near the $\varphi = 90^{\circ}$ plane for the cylinders tested. These are negligible for thin airfoils of any chord.

7. The effect of airfoil and strut shape and size on the noise was shown. Most effects were small; generally blunt trailing edges were quieter.

SYMBOLS

b	effective span of airfoil in the flow, m
c	chord length of airfoil, m
c_o	ambient speed of sound, m/sec
d	thickness of surface normal to flow, m
d_n	nozzle diameter, m
f	frequency or center frequency of third octave band, Hz
f_m	$= (fc/c_o)/(1 - M_o^2)$
F_1, F_2, F_3	functions defined by equation (5)
I_ω	intensity at a given ω, w/m^2
$\overline{I_\omega}$	intensity at $\omega = 2\pi f$, averaged over 1/3 octave band, w/m^2
l_y	transverse scale length defined in reference 8, m
M_o	V_j/c_o, Mach number
$OASPL_c$	overall sound pressure level from SPL_c data, dB
PWL_c	sound power level calculated from SPL_c data (axisymmetric noise), dB
PWL'_c	sound power level from SPL_c data at φ (non-axisymmetric), dB
r	radial distance from nozzle centerline, m
R	microphone radius, m
SPL	sound pressure level, dB

SPL_c	SPL of surface noise only (i.e. jet noise, atmospheric attenuation, tones and background noise removed), dB
$\lvert S_c(\sigma_1, M_o)\rvert^2$	absolute value squared of the two dimensional compressible response function defined in reference 1
T_o	environment temperature, ^oC
T	period, sec
$\sqrt{v^2}/V_i$	transverse turbulence intensity
V_i	impingement velocity (uniform flow), m/sec
V_{ip}	peak impingement velocity (non-uniform flow), m/sec
x	axial location of leading edge of surface from nozzle exit, m
τ	time
α_o	$= 2\ l_y/c$
α	angle of attack, deg.
θ_i	polar angle, measured from inlet to microphone, deg.
ρ_o	ambient density, kg/m^3
φ	azimuthal angle of microphone plane from plane perpendicular to plane of surface and through centerline, deg.
ω	$= 2\pi f$
σ_1	$= \omega c/2V_i = \pi fc/V_i$
ν	kinematic viscosity, m^2/sec

REFERENCES

1. Goldstein, M., Aeroacoustics, McGraw Hill, New York, 1976, Chap. 3.

2. Patterson, R. W., Vogt, P., and Fink, M., "Vortex Noise of Isolated Airfoils," AIAA Paper 72-656, 1972, Boston, Mass.

3. Schlinker, R., Fink, M., and Amiet, R., "Vortex Noise from Non Rotating Cylinders and Airfoils," AIAA Paper 76-81, 1976, Washington, D.C.

4. Lyon, P., Shahady, P., and Elrod, W., "Propeller Acoustic Research (Isolated Airfoil Noise)," AFAPL-TR-75-78, 1975, Air Force Wright Aeronautic Lab, Wright-Patterson Air Force Base, Ohio.

5. Knott, K. R., et al., "Core Engine Noise Control Program. Vol. 2: Identification of Noise Generation and Suppression Mechanisms", August 1974, General Electric Co. (FAA-RD-74-125-Vol-2; AD-A013129/2), Cincinnati, Ohio.

6. Amiet, R., "Acoustic Radiation from an Airfoil in a Turbulent Stream," Journal of Sound and Vibration, Vol. 41, July 1975, pp. 407-420.

7. Goldstein, M. and Atassi, H.: "A Complete Second Order Theory for the Unsteady Flow About an Airfoil Due to a Periodic Gust," Journal of Fluid Mechanics, Vol. 74, 1976, pp. 741-765.

8. Laurence, J.: "Intensity, Scale, and Spectra of Turbulence in Mixing Region of a Free Subsonic Jet," TR-1292, 1956, NASA.

9. Fink, M., "Prediction of Externally Blown Flap Noise and Turbomachinery Strut Noise," August 1975, United Technologies Research Center, East Hartford, Conn.; also CR-134883, NASA.

10. Philips, O., "The Intensity of Aeolian Tones," Journal of Fluid Mechanics, Vol. 1, Dec. 1956, pp. 607-624.

11. Townsend, A. A., "The Structure of Turbulent Shear Flow," Cambridge Univ. Press, 1956, pp. 140, 144.

12. Olsen, W., Miles, J., and Dorsch, R., "Noise Generated by Impingement of a Jet Upon a Large Flat Plate," TN D-7075, 1972, NASA.

13. Goldstein, M., "The Low Frequency Sound from Multipole Sources in Axisymmetric Shear Flows with Applications to Jet Noise," Journal of Fluid Mechanics, Vol. 70, Aug. 1975, pp. 595-604.

14. Goldstein, M., "The Low Frequency Sound from Multi-Pole Sources in Axi-Symmetric Shear Flows, Pt. 2," Journal of Fluid Mechanics, to be published.

15. Olsen, W.: "Advances in Jet and Surface Noise Theory," Lewis Basic Research Review, 1975, pp. 29-31.

16. Boldman, D.: Personal Communication, NASA-Lewis, Cleveland, Ohio.

17. Patterson, R.; Amiet, R.: "Acoustic Radiation and Surface Pressure Characteristics of an Airfoil due to Incident Turbulence," NASA CR to be published under contract NAS1-13823.

18. McKinzie, D.; and Burns, R.: "Large Scale Model EBF Noise Reduction Tests Using Trailing-Edge Blowing and Partial Flap Slot Covering," NASA Technical Note, to be published.

19. Olsen, W. and Karchmer, A., "Lip Noise Generated by Flow Separation from Nozzle Surfaces," AIAA Paper 76-3, 1976, Washington, D.C.

20. McKinzie, D. and Burns, R., "Analysis of Noise Produced by Jet Impingement Near the Trailing Edge of a Flat and a Curved Plate," TM X-3171, 1975, NASA.

TABLE 1. - SURFACES TESTED

Description	Cross section			Spanwise geometry	φ	Other variations
	Sketch on Figure 4	Chord, c, cm	Thickness or diameter d, cm			
I. Circular nozzle with surface in center of mixing region of jet (fig. 3(a)).						
A. Airfoils						
Small chord airfoil	(a-1)	7.9	1.	Straight	0°	
Small chord airfoil	(a-1)	7.9	.32		0°	
Small chord airfoil	(a-2)	8.5 (nominal)			0°-90°	Angle of attack
Large chord airfoil	(a-2)	10.			0°	-
Large chord airfoil	(a-2)	61.			0°	
Infinite chord airfoil	(a-2)	245			0°,90°	
Small chord airfoil	(a-2)	2.5 (nominal)		Ring	axisym-metric	
B. Cylinder	(b-1)	---	2.5 (diam)			
II. Perforated plate nozzle with surface on centerline (fig. 3(b)).						
A. Airfoils						
Small chord airfoil	(a-1)	7.6	2.5	Straight	0°	
Small chord airfoil	(a-1)	1.	1.0		0°,65°	
Large chord airfoil	(a-2)	45,61			0°	← Rough surfaces
(with no LE)	(a-4)	45,61				
(with blunt TE)	(a-3)	45,61			0°,80°	
Infinite chord	(a-2)	245			0°	
(with no LE)	(a-4)	245				
B. Blunt bodies						
1. Cylinder	(b-1)	N/A	0.32,0.64,1.3,2.5,5.1 (d)		0°	
Cyliner	(b-1)	N/A	.64,2.5 (diam.		0°,65°	
2. Half cylinder	(b-2)	N/A	2.5 (diam)		0°	
3. Strip	(b-3)	N/A	2.5 (diam)			
4. Unsymmetrical airfoil (see fig.)	(b-3)	8.9	1.9 (diam)			← Angle of attack

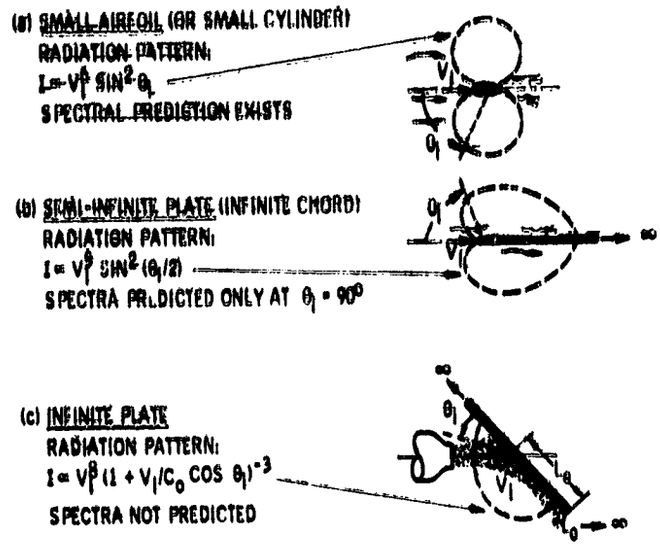

Figure 1. - Simple geometries for which there are basic theories in reference 1.

SURFACES TESTED

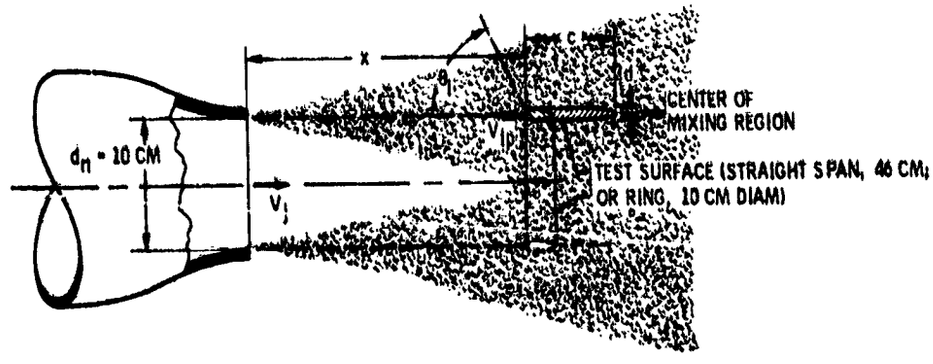

(a) CIRCULAR NOZZLE.

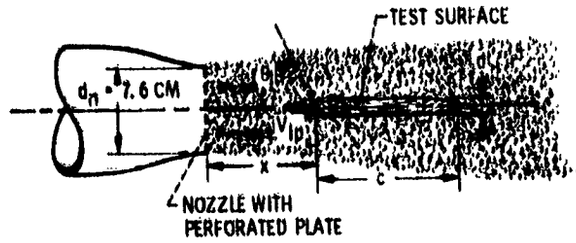

(b) PERFORATED PLATE NOZZLE.

Figure 2 - Nozzles and surface geometries.

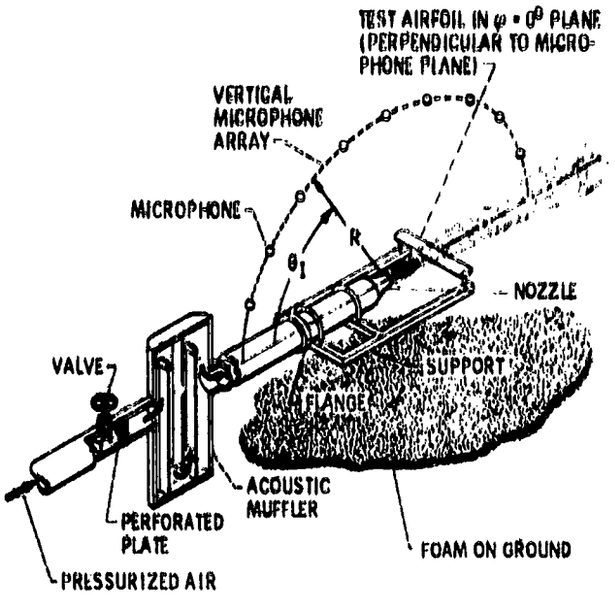

Figure 3. - Flow system, test airfoil and microphone setup.

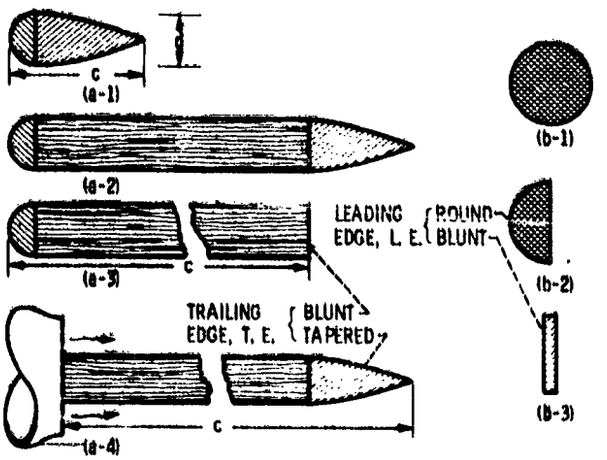

(a) AIRFOILS AND SPLITTERS. (b) BLUNT BODIES.

Figure 4. - Cross sections of the surfaces tested.

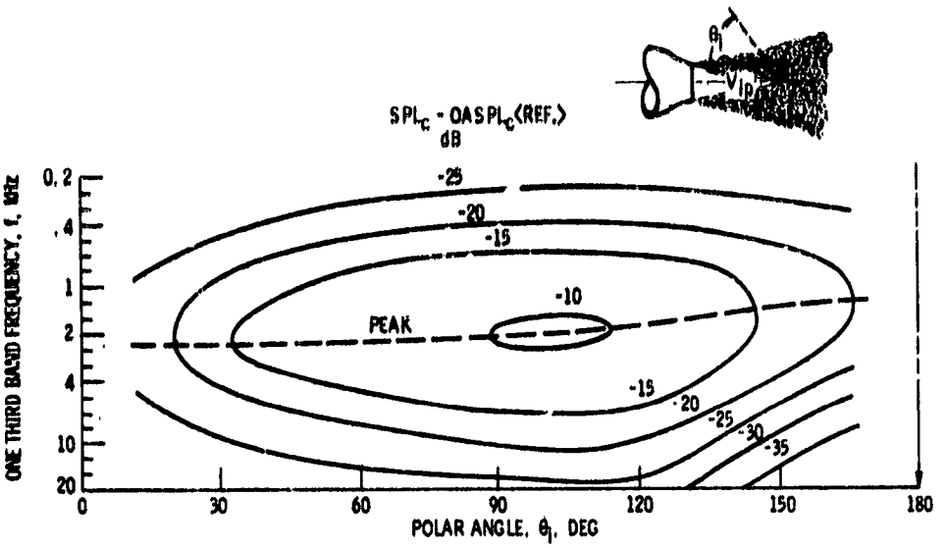

Figure 5. - Smoothed contour plot of noise emission, $SPL_c(f, \theta_1)$, from small chord airfoil. Chord, c, 2.5 cm; peak impingement velocity, V_{jp}, 94 m/sec; azimuthal angle, φ, 0°; free field lossless (ARP 866) data taken on 4.6 m radius; angle for OASPL (ref.); $\theta_1 = 90°$.

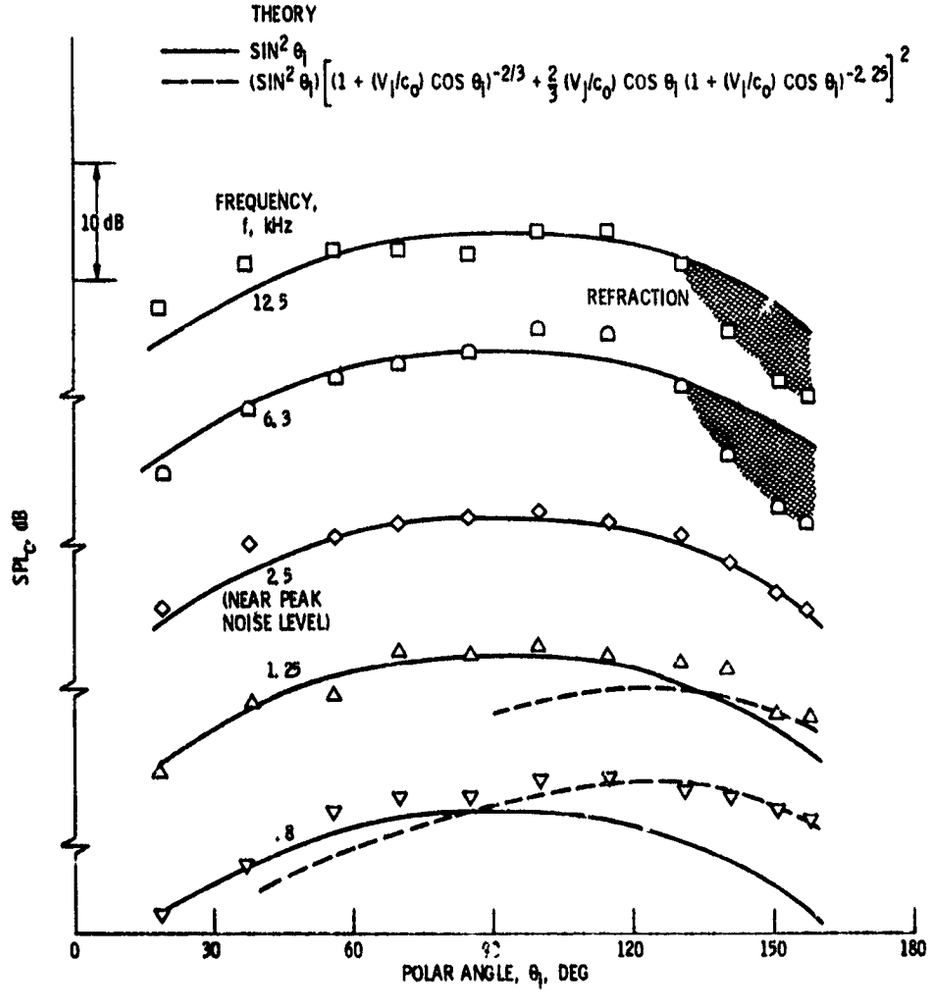

Figure 6. - Shape of radiation pattern at several frequencies. Chord, c, 2.5 cm; impingement velocity, V_{jp}, 94 m/sec; azimuthal angle, φ, 0°; free field lossless data.

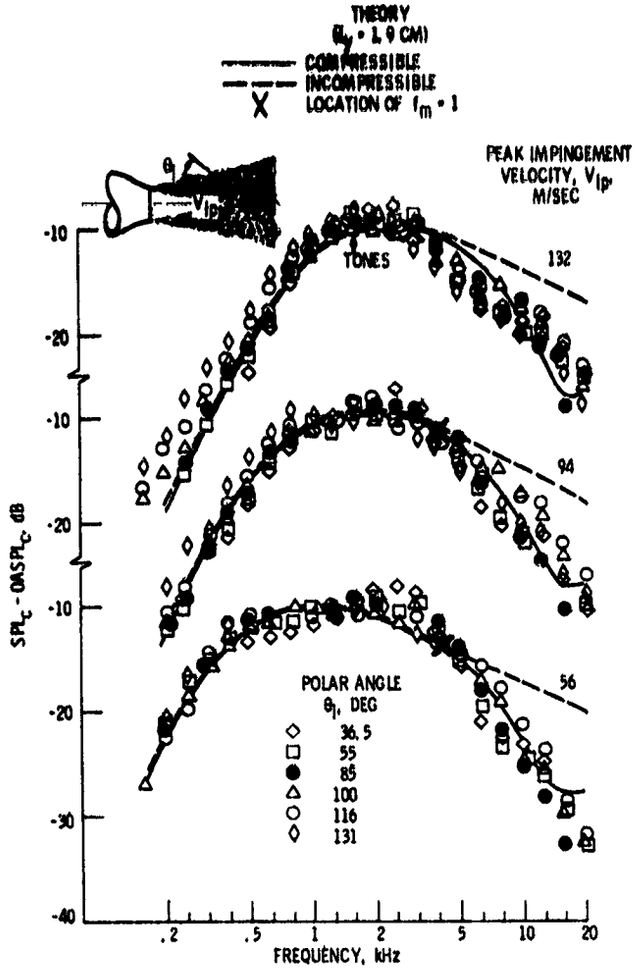

Figure 7. - Effect of angle on the shape of the spectra from a small chord airfoil. Chord, 2.5 cm; azimuthal angle, φ, 0°, free field lossless data.

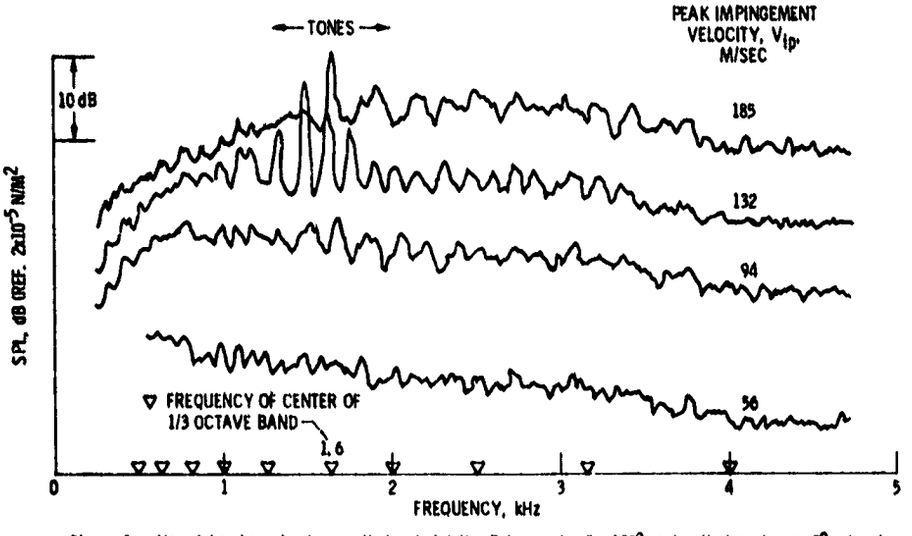

Figure 8. - Narrowband spectra for small chord airfoil. Polar angle, θ_1, 100°; azimuthal angle, φ, 0°; chord, 2.5 cm; airfoil thickness, 0.32 cm; bandwidth, 15 Hz.

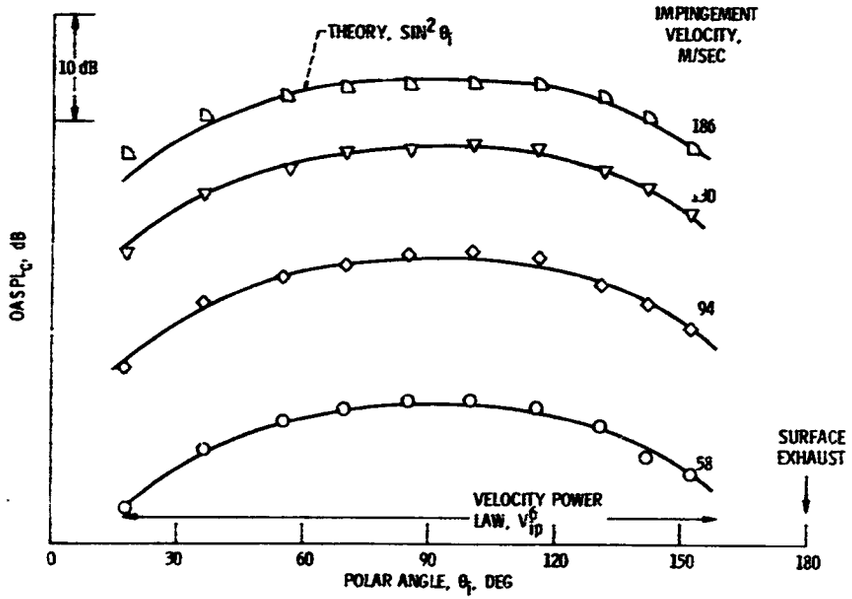

Figure 9. - Radiation pattern of the overall noise from small chord; straight span airfoil, $OASPL_c(\theta_i)$. Chord 2.5 cm; thickness, 0.32 cm; azimuthal angle, φ, 0^0.

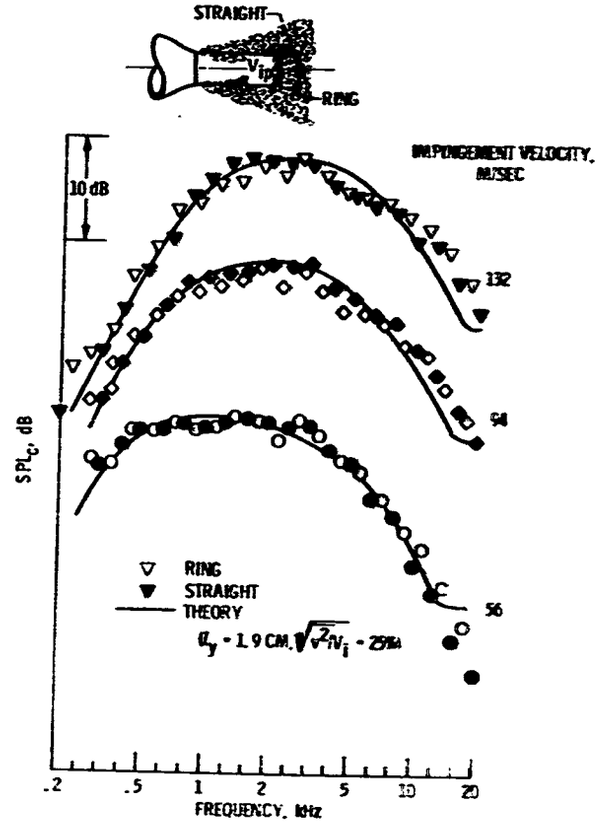

Figure 10. - Comparison of spectra from axisymmetric ring airfoil (uniform impinging flow) and straight airfoil (non-uniform) at $\varphi = 0^0$. Chord, 2.5 cm; polar angle, θ_i, 90^0; free field lossless data.

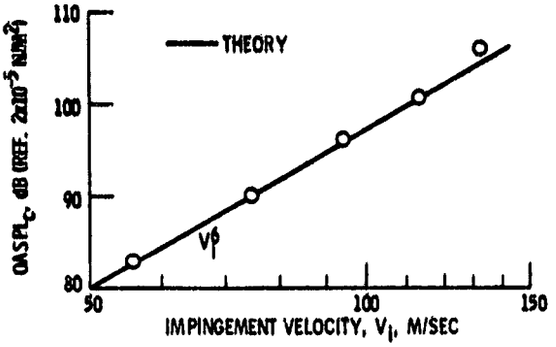

Figure 11. - Absolute level of noise from ring airfoil. Polar angle, θ_j, 90°; chord, c, 2.54 cm; distance, R, 4.6 m; ring diameter, 10 cm; turbulence scale, L_y, 1.9 cm; turbulence intensity, 25%; environmental temperature, 16° C.

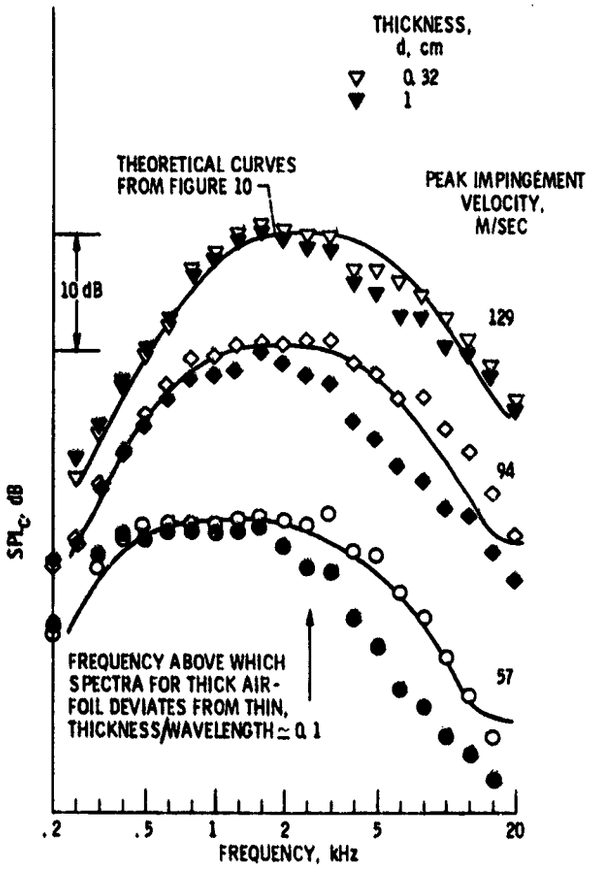

Figure 12. - Effect of airfoil thickness on spectra for small chord airfoil. Chord, c, 2.5 cm; polar angle, θ_j, 100°; free field lossless data.

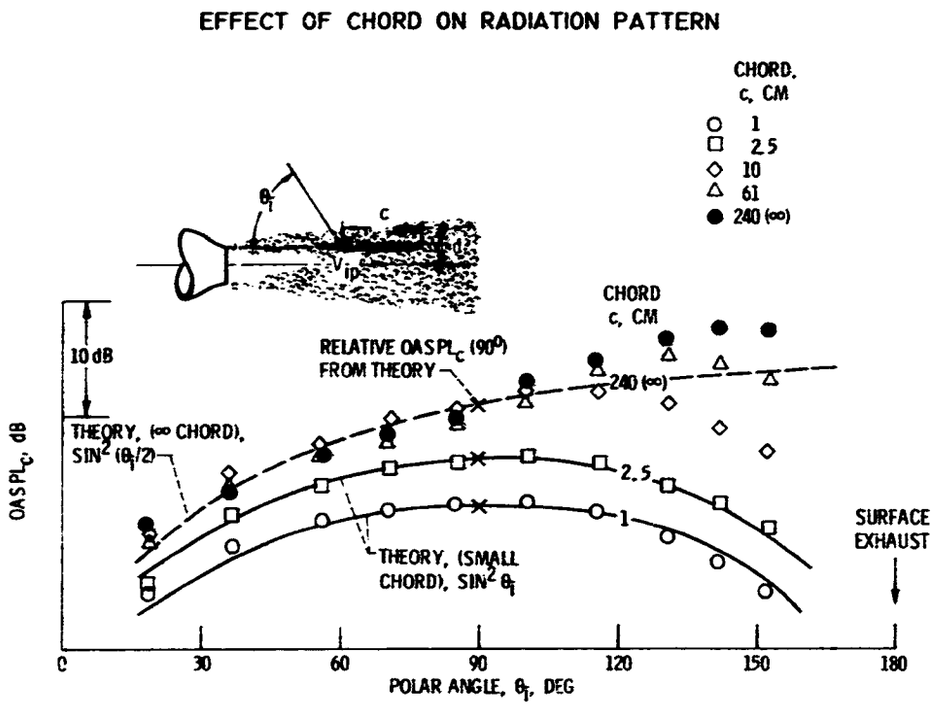

Figure 13. - Effect of chord length on the radiation pattern from thin airfoils. Impingement velocity, V_{ip}, 94 m/sec; airfoil thickness, d, 0.32 cm; location of fixed leading edge $x = 4 d_n = 0.4$ m; free field lossless data.

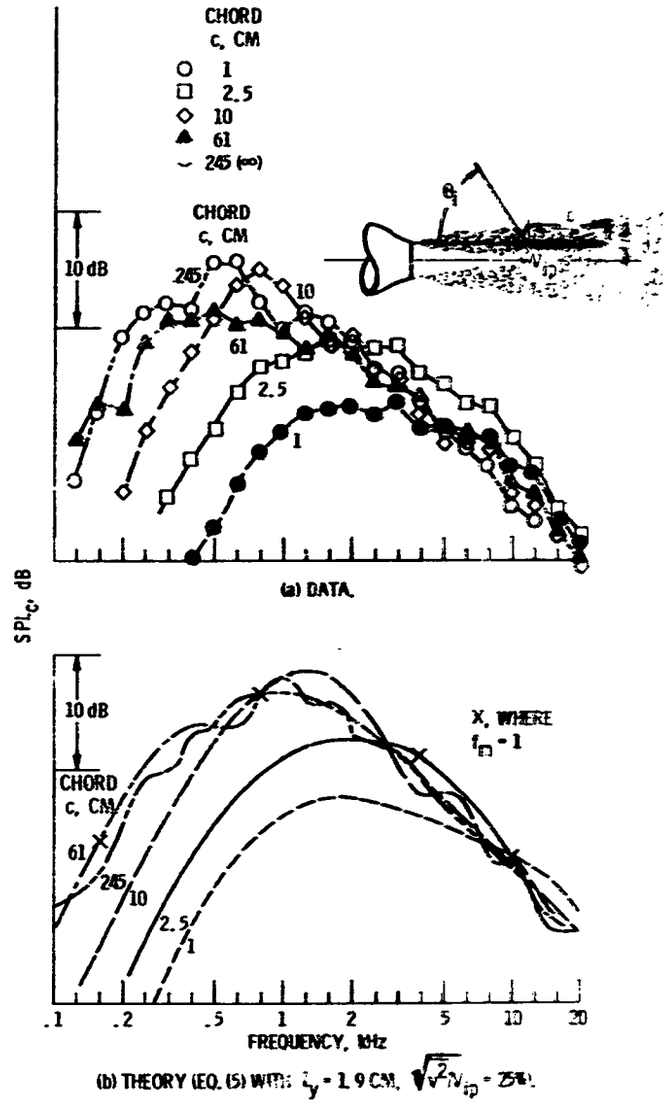

(b) THEORY (EQ. (5)) WITH ℓ_y = 1.9 CM, $\sqrt{v^2}/V_{ip}$ = 25%.

Figure 14. - Effect of airfoil chord length on spectra at $\theta_i = 90°$. Peak impingement velocity, V_{ip}, 94 m/sec; airfoil thickness, d, 0.32 cm; azimuthal angle, Φ, 0°; free field lossless data.

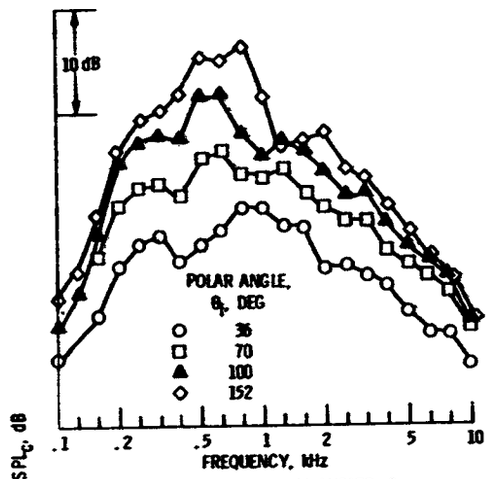

(a) SPECTRA AT SEVERAL ANGLES, θ_f

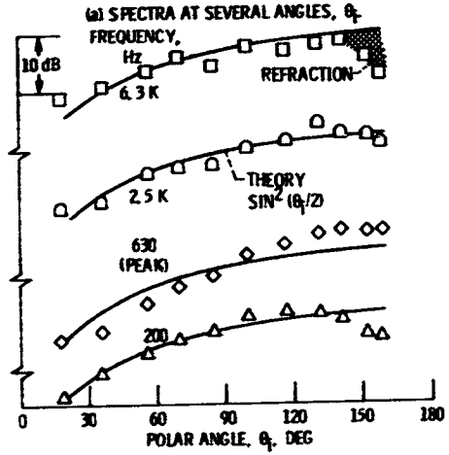

(b) SPL RADIATION PATTERN AT SEVERAL FREQUENCIES.

Figure 15. - Noise emission from an infinite chord airfoil. Impingement velocity, V_{ip}, 94 m/sec; chord, c, 245 cm; airfoil thickness, 0.32 cm; azimuthal angle, φ, 0°, free field lossless data at 4.6 m.

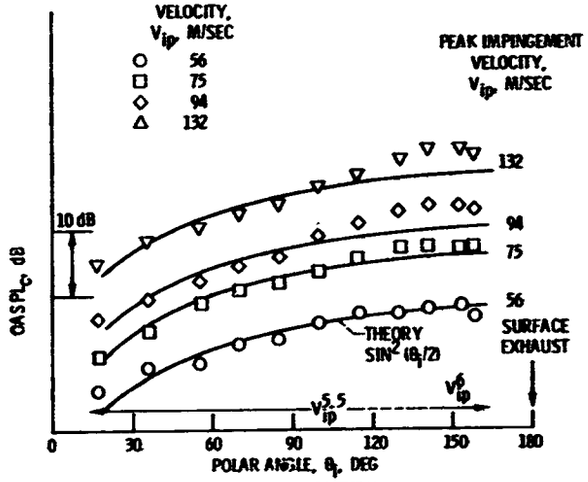

(a) RADIATION PATTERN.

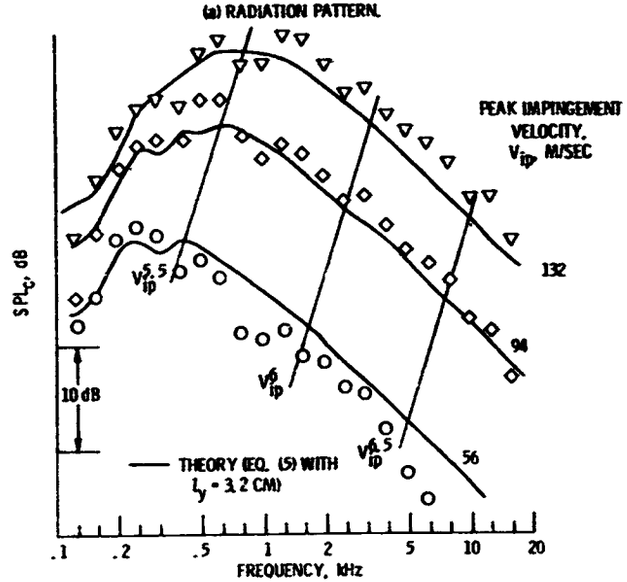

(b) SPECTRA AT θ_f = 90°.

Figure 16. - Noise emission from an infinite chord airfoil. Chord, 245 cm; airfoil thickness, 0.32 cm; azimuthal angle, φ, 0°; free field lossless data at 4.6 m.

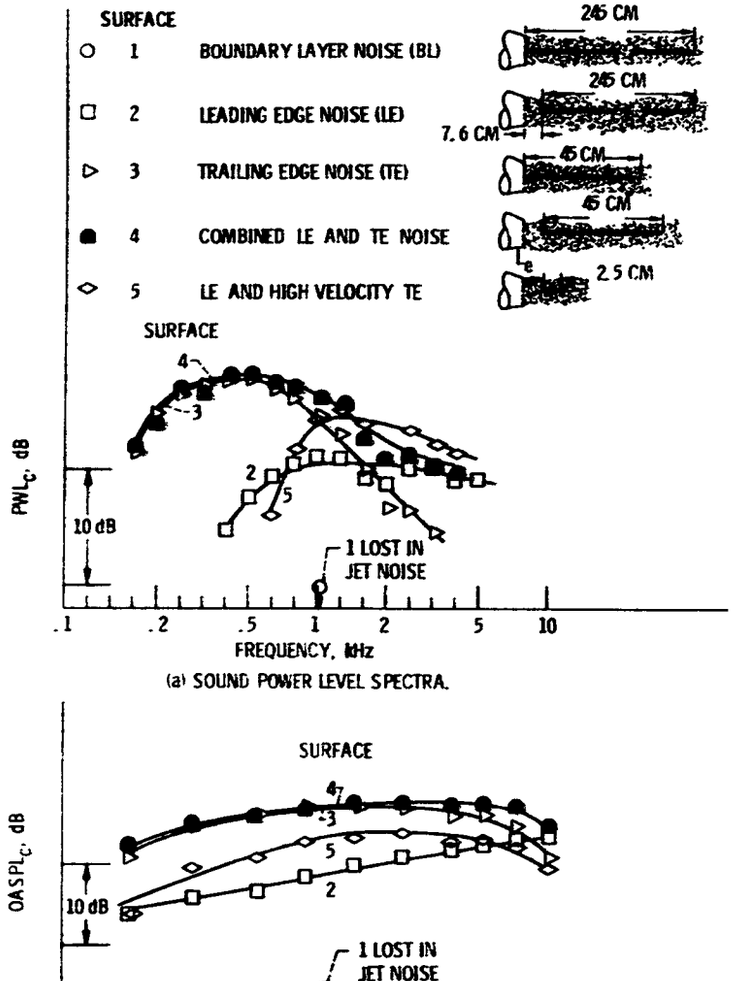

Figure 17. - Separation of leading edge trailing edge and boundary layer noise. Peak velocity at leading edge location, V_{ip}, 115 m/sec; airfoil thickness, 1 cm; azimuthal angle, φ, 0°; free field lossless data.

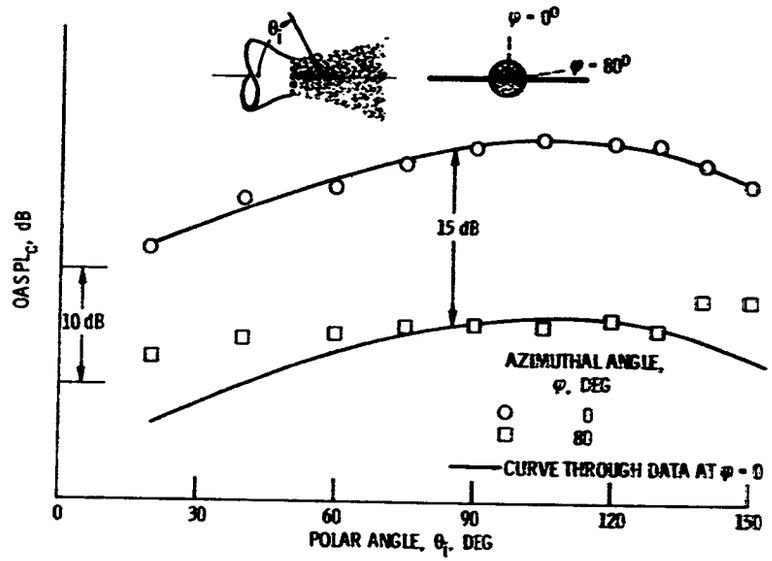

Figure 18. - Airfoil drag dipole investigation. Peak impingement velocity, V_{ip}, 172 m/sec; airfoil thickness, 1 cm; chord, 2.5 cm; free field lossless data.

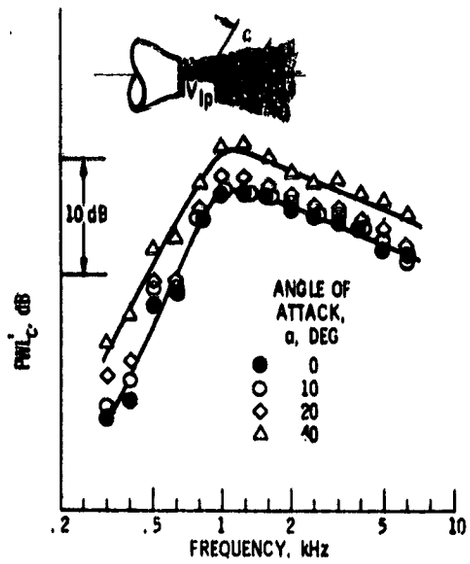

Figure 19. - Effect of airfoil angle of attack on noise. Peak impingement velocity, V_{ip}, 172 m/sec; airfoil chord, c, 8.9 cm; thickness, d, 1.9 cm; azimuthal angle, φ, 0^0; lossless data corrected to free field.

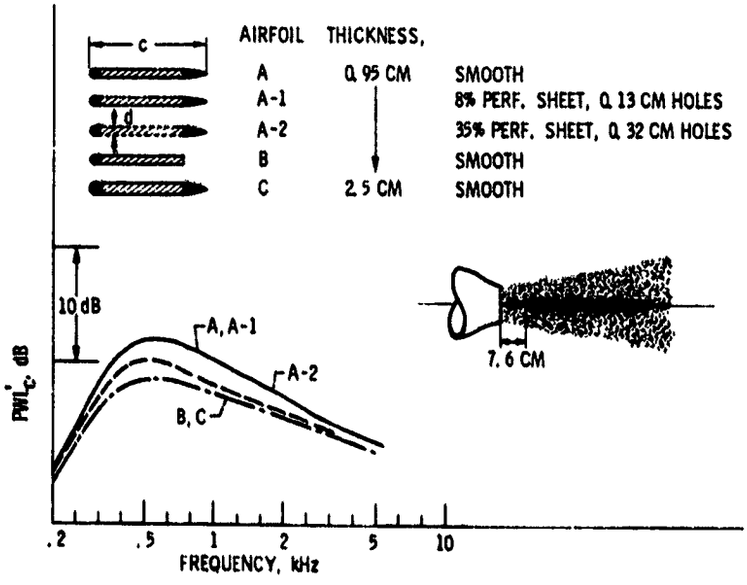

Figure 20. - Effect of variations in geometry and surface roughness on noise from a long chord airfoil. Impingement velocity, V_{ip}, 172 m/sec; chord, c, 45 cm; azimuthal angle, φ, 0^0; lossless data corrected to free field.

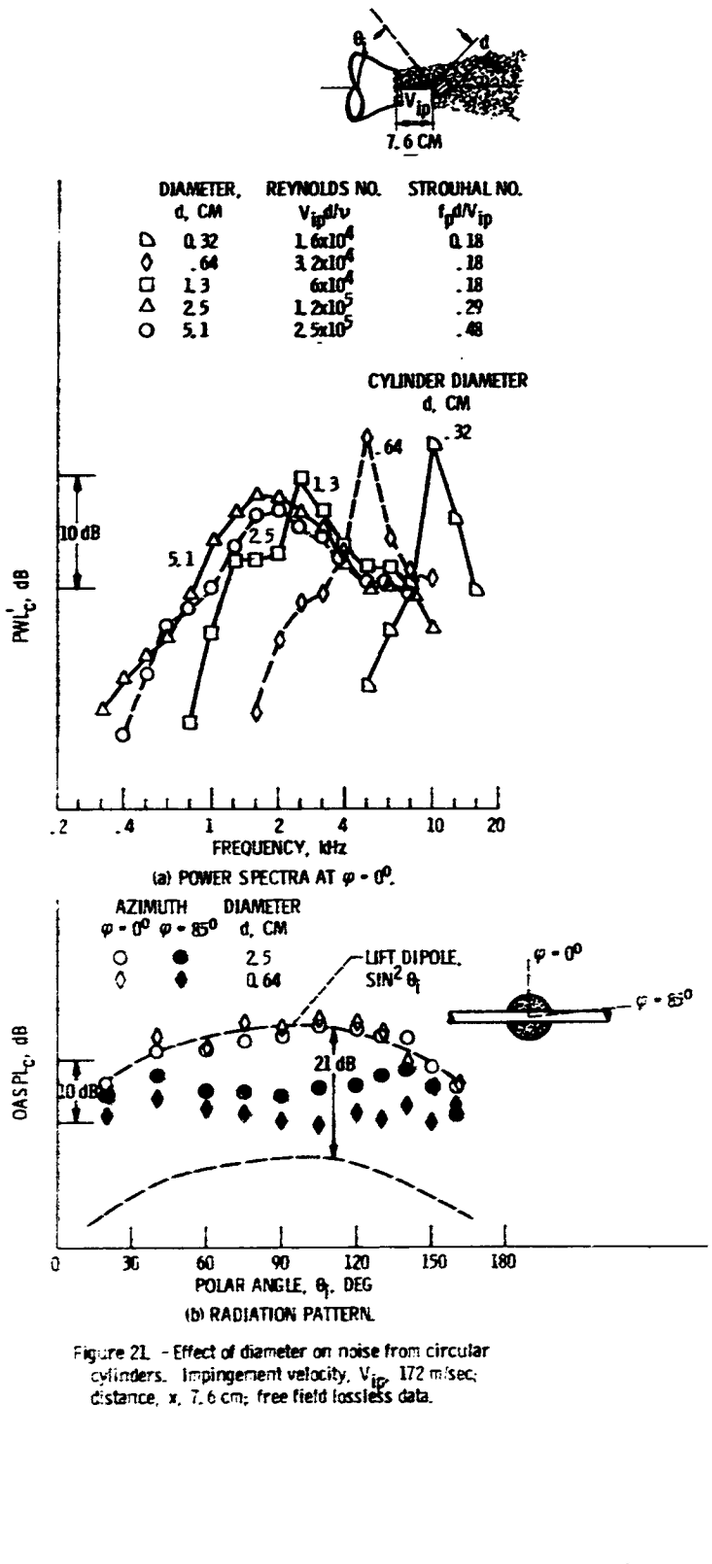

Figure 21. - Effect of diameter on noise from circular cylinders. Impingement velocity, V_{ip}, 172 m/sec; distance, x, 7.6 cm; free field lossless data.

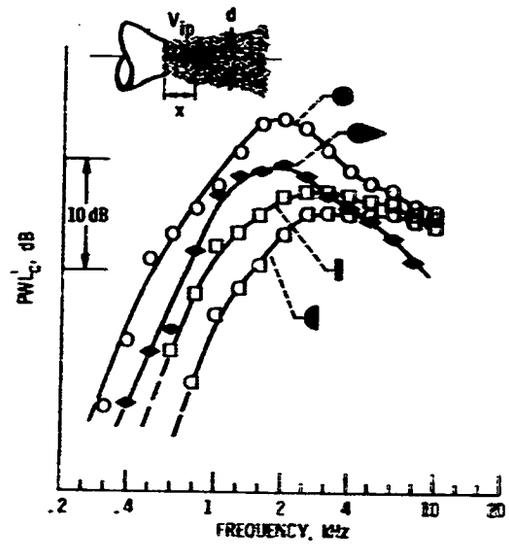

Figure 22. - Effect of cross sectional shape. Peak impingement velocity, V_{ip}, 172 m/sec; thickness, d, 2.5 cm; Reynolds no. $1.2x10^5$; azimuthal angle, φ, 0°; lossless data corrected to free field.